Optical absorption spectra of the uranium (4+) ion in the thorium germanate matrix

1997 J. Phys.: Condens. Matter 9 557

(http://iopscience.iop.org/0953-8984/9/2/023)

J. Phys.: Condens. Matter **9** (1997) 557–567. Printed in the UK PII: S0953-8984(97)76831-0

Optical absorption spectra of the uranium (4+) ion in the thorium germanate matrix

Z Gajek†, J C Krupa‡ and E Antic-Fidancev§

† W Trzebiatowski Institute of Low Temperature and Structure Research, Polish Academy of Sciences, 50-950 Wrocław, PO Box 937, Poland

‡ Laboratoire de Radiochimie, Institut de Physique Nucléaire, BP 1, 91406 Orsay Cédex, France

§ Unité P- de Recherche associée au CNRS 210, 1 place A Briand, 92195 Meudon Cédex, France

Received 31 July 1996, in final form 15 September 1996

Abstract. Visible and infrared absorption measurements on the U^{4+} ion in tetragonal zircon-type matrix β-$ThGeO_4$ are reported and analysed in terms of the standard parametrization scheme. The observed 17 main peaks and a number of less intense lines have been assigned and fitted to most of the 32 allowed electric dipole transitions with the root mean square error equal to 65 cm^{-1}. The free-ion parameters obtained for the model Hamiltonian, $\zeta_{5f} = 1809$ cm^{-1}, $F^2 = 43\,065$ cm^{-1}, $F^4 = 38\,977$ cm^{-1} and $F^6 = 24\,391$ cm^{-1}, as well as the corresponding crystal-field parameters, $B_0^2 = -1790$ cm^{-1}, $B_0^4 = 1200$ cm^{-1}, $B_4^4 = 3260$ cm^{-1}, $B_0^6 = -3170$ cm^{-1} and $B_4^6 = 990$ cm^{-1}, agree fairly well with the initial theoretical estimations. The results are discussed in relation to the previous spectroscopic study on the scheelite-type matrix $UGeO_4$.

1. Introduction

The tetragonal β-$ThGeO_4$ matrix doped with an f-electron element belongs to the group of compounds which can be considered for potential applications in modern laser or luminescent material technologies. On the other hand, the specificity of the oxygen environment of the actinide ion and the relatively low symmetry of this in the zircon structure matrix is interesting from the viewpoint of electronic properties of the actinide ion bonding. The present paper reports optical absorption spectra recorded for β-$ThGeO_4$:U^{4+} in the visible and infrared regions at various temperatures. The spectra are discussed on the grounds of the model of electronic energy levels for the U^{4+} ion in a one-electron crystal field potential. Our phenomenological Hamiltonian has a conventional parametric form and the standard least-squares fitting procedure is employed [1]. Previous studies on the similar compounds β-$ThSiO_4$:U^{4+} [2] and $UGeO_4$ [3] serve as a guideline and instructive reference in this work. The area of physically acceptable solutions is marked out by the consistent predictive model (CPM) proposed by Crosswhite and Crosswhite [4], Carnall and Crosswhite [5] and Krupa [1] for the free-ion parameters and the theoretical estimation of the crystal-field parameters based on the first-principles perturbative model (FPPM) [6]. In addition, the preliminary estimation of the crystal-field effect is provided by the angular overlap model (AOM) simulation [7]. Details concerning both the measurements and the calculations as well as the results obtained are described in the next three sections. The

0953-8984/97/020557+11$19.50

discussion presented in section 5 concerns limitations of the proposed interpretation of the spectra, comparison with the referenced data and some characteristic features of the tetragonal matrix under study. Main conclusions are gathered in section 6.

2. Experimental details

Thorium germanate crystallizes in two forms: the scheelite-type structure α ($CaWO_4$) and the zircon-type structure β [8]. A polycrystalline high-temperature β-phase of the sample of $ThGeO_4$ has been obtained by the flux growth method using Li_2MoO_4 as a melting salt at a temperature of 1150 °C. X-ray powder diffraction analysis has shown the product to be a single phase that could be indexed in the D_{4h}^{19} space group with the lattice constants in good agreement with those found by Ennaciri *et al* [8]. The uranium ion is surrounded by eight oxygen atoms forming two interpenetrating tetrahedra: elongated tetrahedra and flattened tetrahedra twisted mutually by the 90° angle. According to the crystallographic data obtained by Ennaciri *et al* [8] the U–O distances are equal to 2.473 Å (elongated) and 2.358 Å (flattened) which can be compared with the value of 2.369 Å observed for UO_2 [9]. The exact point symmetry at the uranium site is D_{2d}. The uranium energy levels can be labelled in terms of five irreducible representations of the D_{2d} point group: four singlets Γ_1, Γ_2, Γ_3, Γ_4 and one doublet Γ_5. The allowed electric dipole (ED) transitions are shown in table 1. The degenerate $5f^2$(SL)J terms split into 70 levels: $16\Gamma_1+9\Gamma_2+12\Gamma_3+12\Gamma_4+21\Gamma_5$, i.e. 49 singlets Γ_1, Γ_2, Γ_3, Γ_4 and 21 doublets Γ_5.

Table 1. Selection rules for electric dipole transitions in the system of D_{2d} symmetry. The symbols σ and π denote the polarization of the radiation field.

	Γ_1	Γ_2	Γ_3	Γ_4	Γ_5
Γ_1				π	σ
Γ_2			π		σ
Γ_3		π			σ
Γ_4	π				σ
Γ_5	σ	σ	σ	σ	π

The optical absorption spectra were recorded from 2600 to 400 nm at 300, 40 and 9 K. The low-temperature recordings are shown in figure 1. As seen, they contain broad structures more characteristic for solid $UGeO_4$ rather than for doped compounds. One can easily distinguish eight typical $U^{4+}(5f^2)$ bands which are closely related to the free-ion groups of f^2(LS)J levels. Table 2 shows the correlation between these bands and the CPM free-ion states. The maximum numbers of ED transitions that can be observed for each of the bands depend on the ground state and they are shown in table 2 as well.

There are two energy regions, 8500–10 500 cm^{-1} and 14 500–17 000 cm^{-1}, of a relatively high (SL)J state density. Figure 1 shows that the spectra of β-$ThGeO_4$:U^{4+} and $UGeO_4$ differ markedly in these regions. This inclined us to exclude them at the beginning of the fitting procedure. Review of the available literature data shows that actinide ions in a tetrahedral oxygen environment display a large variety of electronic properties, especially regarding the crystal-field effect (see, e.g., [1]). Therefore we examine several different assignments of the spectra within different electronic structure models. In each case the stability of the solutions has been checked by varying the parameters obtained within their uncertainty limits.

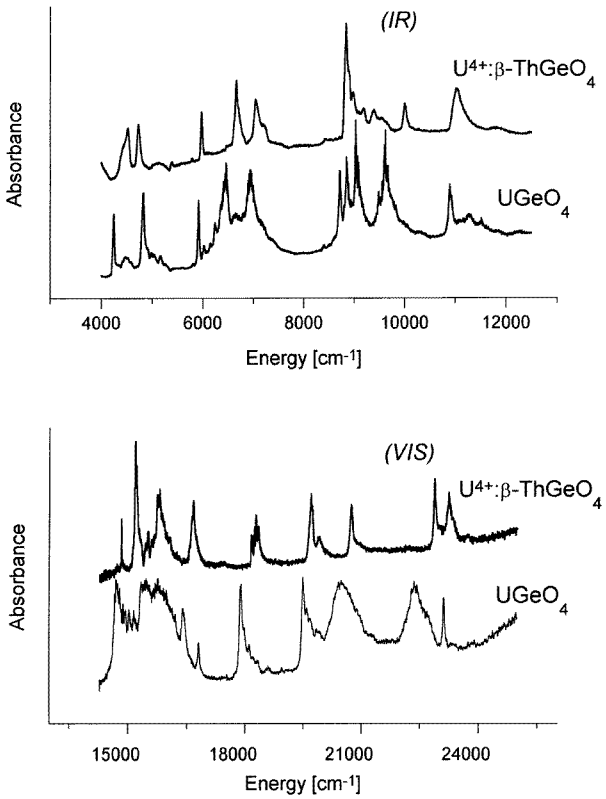

Figure 1. Comparison of the absorption spectra of $UGeO_4$ [3] and β-$ThGeO_4$:U^{4+} in the infrared (IR) and visible (VIS) regions.

3. Initial estimation of the electronic structure parameters

The model Hamiltonian defined for the $5f^2$ electronic structure function space employed in our analysis of the spectra consists of two parts. The free-ion part may be written as

$$H_0 = \sum_{k=0,2,4,6} F^k \mathbf{f}_k + \zeta_{5f} \sum_i \mathbf{l}_i \cdot \mathbf{s}_i + \alpha L(L+1) + \beta \mathbf{G}(G_2) + \gamma \mathbf{G}(R_7) + \sum_{k=0,2,4} M^k \mathbf{m}_k + \sum_{k=2,4,6} P^k \mathbf{p}_k \quad (1)$$

where the first two terms describe the Coulomb repulsion of the f electrons and the spin–orbit interaction and the remaining terms represent the higher-order corrections due to the configuration interaction [10]. Each of the quantities in (1) is written and defined according to conventional practice [1].

The physicochemical correctness of the most important parameters in H_0, F^k and ζ indicates their general regularity along the elements of the whole $5f^N$ series according to the CPM. We are looking for solutions of the experimental data fits that do not differ essentially from the CPM values $\zeta \simeq 1810$ cm^{-1}, $F^2 \simeq 42\,900$ cm^{-1}, $F^4 \simeq 39\,900$ cm^{-1} and $F^6 \simeq 25\,600$ cm^{-1} [1]. The higher-order parameters in H_0 have not been varied except for the parameter α and, in the initial trials, M^0.

Table 2. Absorption regions characteristic of U^{4+} ion in a tetragonal matrix of D_{2d} symmetry, the corresponding *free-ion* energy levels (calculated with the CPM parameters quoted in section 3) and the numbers of allowed ED transitions for different ground states.

	Energy interval (cm^{-1})	*Free-ion* levels (cm^{-1}) and main SLJ components	Number of ED transitions for the following ground states			
			Γ_1, Γ_2	Γ_3	Γ_4	Γ_5
I	4000–5500	4430 ($^3F_2$)	2	1	2	4
II	5500–8500	6610 ($^3H_5$)	4	5	4	8
III	8500–10 500	8960 ($^3F_3$), 9650 ($^3F_4 + {}^1G_4$)	6	6	6	12
IV	10 500–12 000	11 510 ($^3H_6$)	5	4	5	10
V	14 500–17 000	15 190 ($^1D_2 + {}^3P_2$), 15 210 ($^3P_0$), 16 370 ($^3F_4 + {}^1G_4$)	5	4	7	12
VI	17 500–19 000	17 790 ($^3P_1$)	1	2	1	2
VII	19 000–21 500	20 630 ($^1I_6$)	4	4	5	8
VIII	21 500–23 500	22 460 ($^3P_2 + {}^1D_2$)	3	1	2	6
	Total number of transitions		30	27	32	62

The phenomenological D_{2d} crystal-field potential acting on electron i has in conventional notation the following form:

$$V(i) = \sum_{k,q} B_q^k \mathbf{C}_q^k(i) \tag{2}$$

where $k = 2, 4, 6$; $q = 0, \pm 4$; $q \leqslant k$, $B_{-q}^k = B_q^k = (B_q^k)^*$. The parameters B_q^k are given by two independent theoretical approaches:

(i) the FPPM [6] and
(ii) the semiempirical AOM [7].

Both models indicate the order of the expected crystal-field parameters. Model (i) stems from many-body perturbation theory for non-orthogonal basis states and the one-electron approximation of the effective Hamiltonian [6, 11]. It has been applied successfully to a number of lanthanide and actinide compounds [12]. The model allows one to understand the subtle crystal-field properties and gives an insight into the particular physicochemical mechanisms involved. The most important of these are listed in table 3. Besides the classical electrostatic contributions such as point charges, the correction due to the spatial distribution of the ligand electrons (the Kleiner correction) and the influence of induced multipoles, the model takes into account the inter-ion exchange interaction, the renormalization contributions due to the non-orthogonality of the free-ion orbitals (overlapping and contact shielding) and the charge-transfer effect (covalency). Details of the calculations can be found in [6].

The second approach (ii) allows one to see the crystal-field effect from the viewpoint of the strength of the individual metal–ligand (M–L) interaction. If $V(\boldsymbol{r}-\boldsymbol{R})$ is an effective potential of a single ligand placed at $\boldsymbol{R}$ that acts on an f electron at point $\boldsymbol{r}$, then $e_\sigma = \langle m = 0|V|m = 0\rangle_R$, $e_\pi = \langle m = \pm 1|V|m = \pm 1\rangle_R$ and $e_\delta = \langle m = \pm 2|V|m = \pm 2\rangle_R$ are the effective AOM parameters describing the M–L interaction. The subscript $\boldsymbol{R}$ to the angular bracket $\langle \ldots \rangle_R$ indicates the quantization axis. The AOM parameters are related to

Table 3. Comparison of various sets of crystal-field parameters for the U^{4+} ion.

	B_0^2 (cm^{-1})	B_0^4 (cm^{-1})	B_4^4 (cm^{-1})	B_0^6 (cm^{-1})	B_4^6 (cm^{-1})
AOM for β-$ThGeO_4$	−192	1824	−4700	−2256	256
FPPM calculations for β-$ThGeO_4$	26	1644	−3463	−1649	64
Point charges—nearest neighbours	312	1686	−4475	−1264	153
Kleiner correction	41	−1318	3346	1727	−319
Exchange	21	−1221	3147	1722	−214
Overlapping	−607	2842	−7208	−3622	599
Covalency	−325	538	−1271	−219	173
Contact shielding	−1	81	−209	−81	9
Induced dipoles—nearest neighbours	1390	208	2440	509	−404
Point charges—further neighbours	−841	−1261	780	−422	76
Induced dipoles—further neighbours	36	85	−12	2	−9
AOM for α-$ThGeO_4$	784	−3232	−4576	−832	−2624
FPPM calculations for α-$ThGeO_4$	−158	−2439	−6341	195	−218
$UGeO_4$: model A [3]	−1782	2521	−3061	−3806	−504
$UGeO_4$: model B [3]	2918	−2051	−3026	−487	−1986
α-$ThSiO_4$ [2]	−1003	1147	−2698	−2889	−208

[a] See [6] for further details concerning the particular contributions provided by the FPPM.

the usual crystal-field parameters as follows:

$$B_q^k = \frac{2k+1}{7}\left[\begin{pmatrix} 3 & k & 3 \\ 0 & 0 & 0 \end{pmatrix}\right]^{-1} \sum_{\mu=0,\pm 2} \begin{pmatrix} 3 & k & 3 \\ -\mu & 0 & \mu \end{pmatrix} \sum_t e_\mu(t) C_q^{k*}(t) \qquad (3)$$

where t runs over the ligands.

This old, frequently forgotten model allows one to deduce the crystal-field splitting on the ground of the available data for a given M–L bond in other crystals, in a similar way to the more common superposition model [13]. The characteristic order of the AOM parameters, $e_\sigma > e_\pi \approx e_\sigma/3 > (>) e_\delta$, observed for f-electron elements [7] justifies the use initially of the simplest one-parameter version, AOM-I, defined by the following constraints: $e_\pi = e_\sigma/3$ and $e_\delta = 0$. This model predicts definite ratios between the intervals of the crystal-field levels. The AOM set of the crystal-field parameters listed in table 3 has been obtained using $e_\sigma = 1600$ cm^{-1}, i.e. a value consistent with the crystal-field interpretation for UO_2 [14], and M–L distance dependence factors estimated by means of squares of interatomic overlap integrals [7].

As seen from table 3, our two independent predictions are convergent at least for the most relevant fourth-order parameters. The same is true for the scheelite form of the germanate; the results obtained for this are also presented in table 3 for comparison.

4. Phenomenological analysis

All the theoretical sets of crystal-field parameters listed in table 3 together with the free-ion CPM parameters have been used as starting parameters in our data fits. Other starting sets applied were those obtained previously for $UGeO_4$ [3] and $ThSiO_4$:U^{4+} [2]. As a result of the fitting, we have obtained two different and stable solutions, namely model A and model B, characterized by similar root mean square error of the order of 65 cm^{-1}. The two solutions differ mainly in the crystal-field parameters. One of them, model A, is

consistent with our theoretical predictions for β-$ThGeO_4$:U^{4+} and therefore it is accepted as an actual interpretation. It is interesting to note that model B coincides with theoretical results obtained for the scheelite matrix α-$ThGeO_4$. Further discussion concerns mainly model A.

The number of observed levels included in the final data fits in model A was 23 and the number of parameters allowed to vary was ten. The structures observed at 8974 and 16 675 cm^{-1} were treated as complex and composed of Γ_2 and Γ_5 pairs. A list of the observed and calculated energy levels and their compositions are shown in table 4. Those allowed by the ED selection rules are indicated in the observed absorption spectra (figure 2). The model parameters provided by both the fittings, A and B, are listed in table 5.

5. Discussion

As seen from figure 2 and table 4 model A provides a satisfactory description of the most of the observed absorption bands. There are, however, some exceptions that cannot be fully explained at the present stage. One exception concerns the structure at 4350–4530 cm^{-1} which seems to be complex, contrary to the selection rules which predict only one transition in this region. The same is true for the comb structure at 18 282 cm^{-1}. Instead of one peak we observe at least five lying very close to each other. This indicates that there are several non-equivalent positions of the uranium ion. Probably the system may respond to the smaller ionic radius of the uranium ion in comparison with the thorium ion in several ways. The existence of non-equivalent uranium sites is confirmed by preliminary laser selective excitation measurements. This may also be seen as one of the mechanisms responsible for the broadening of the structures observed at 11 030, 15 744, 15 808, 16 675 and 23 241 cm^{-1}.

The situation becomes more complicated, however, if one takes into account in the above context the other lines of the spectra which remain relatively narrow. Are the corresponding electronic levels so much less sensitive to changes in the uranium environment? For the present there is no adequate model of the metal neighbourhood rearrangement caused by the doped ion. The literature provides, however, an instructive example of the incommensurate phase of the β-$ThCl_4$ [16]. In this phase a continuous variation in the uranium ion environment due to the transverse displacement of the chlorine ions is observed. The high-temperature phase symmetry D_{2d} is broken below 70 K to S_4, D_2, C_2 according to the modulation phase. It has been shown that the character of the energy variation with the displacement changes essentially from level to level. In general, the levels originating from the Γ_5 level in the high-temperature phase turned out to be more sensitive than the others. Coming back to the germanate matrix we can only note that the supposed non-equivalent positions of the uranium ion differ rather slightly from each other and we observe some average effect.

The most apparent changes in the position of Γ_5 ($^3P_1$) are determined solely by the B_0^2 parameter, the value of which is not very well resolved in the data fits. The FPPM calculations for B_0^2 show that there are two contributions which are similar but of opposite sign and originate from the two coordination tetrahedra. The competition between these results in a small positive value of this parameter. The equilibrium, however, may be easily broken even by a slight displacement of the chlorine ions to gain large changes in B_0^2.

Less intense lines at 7806, 9383 and 19 966 cm^{-1} may be attributed to the phonon-assisted transitions with phonon energies equal to 150 cm^{-1}, 537 cm^{-1} and 210 cm^{-1}, respectively. Similar frequencies have been observed for $UGeO_4$. They are also consistent with the detailed analysis of the vibration infrared and Raman spectra reported for α-$ThGeO_4$ [17] according to which the most efficient in the energy range 150–600 cm^{-1} are

Table 4. Calculated and experimental energy levels of U^{4+} in β-$ThGeO_4$ with the main $|S, L, J, M_J\rangle$ components of the eigenvectors.

Γ	E^{a}_{calc} (cm^{-1})	E_{obs} (cm^{-1})	ΔE (cm^{-1})	Eigenvector
4	0	0	0	$-0.67\|1, 5, 4, -2\rangle + 0.67\|1, 5, 4, 2\rangle$
5	208	$\simeq 184^{b}$	24	$0.83\|1, 5, 4, -1\rangle - 0.40\|1, 5, 4, 3\rangle$
1	434	—		$-0.83\|1, 5, 4, 0\rangle - 0.32\|0, 4, 4, 0\rangle$
2	1256	—		$0.66\|1, 5, 4, -4\rangle - 0.66\|1, 5, 4, 4\rangle$
3	1270	—		$0.68\|1, 5, 4, -2\rangle + 0.68\|1, 5, 4, 2\rangle$
1	1280	—		$-0.43\|1, 5, 4, 0\rangle - 0.59\|1, 5, 4, -4\rangle - 0.59\|1, 5, 4, 4\rangle$
5	1539	—		$-0.42\|1, 5, 4, -1\rangle - 0.83\|1, 5, 4, 3\rangle$
3	4016	—		$-0.63\|1, 3, 2, -2\rangle - 0.63\|1, 3, 2, 2\rangle$
5	4284	4378	−94	$-0.84\|1, 3, 2, -1\rangle - 0.34\|0, 2, 2, -1\rangle$
4	4367	—		$-0.64\|1, 3, 2, -2\rangle + 0.64\|1, 3, 2, 2\rangle$
1	4698	4733	−35	$0.90\|1, 3, 2, 0\rangle + 0.36\|0, 2, 2, 0\rangle$
3	5821	—		$0.69\|1, 5, 5, -2\rangle - 0.69\|1, 5, 5, 2\rangle$
5	6023	5977	46	$-0.73\|1, 5, 5, -1\rangle + 0.49\|1, 5, 5, 3\rangle$
2	6051	—		$-0.88\|1, 5, 5, 0\rangle$
4	6727	—		$0.67\|1, 5, 5, -2\rangle + 0.67\|1, 5, 5, 2\rangle$
5	6756	6658	98	$-0.44\|1, 5, 5, -1\rangle - 0.80\|1, 5, 5, 3\rangle + 0.32\|1, 5, 5, -5\rangle$
1	7075	7056	19	$-0.69\|1, 5, 5, -4\rangle + 0.69\|1, 5, 5, 4\rangle$
5	7147	7206	−59	$-0.39\|1, 5, 5, -1\rangle - 0.86\|1, 5, 5, -5\rangle$
2	7157	—		$0.45\|1, 5, 5, 0\rangle + 0.61\|1, 5, 5, -4\rangle + 0.61\|1, 5, 5, 4\rangle$
4	8568	—		$-0.56\|1, 3, 3, -2\rangle - 0.56\|1, 3, 3, 2\rangle$
5	8760	8846	−86	$0.90\|1, 3, 3, 3\rangle$
3	8946	—		$-0.66\|1, 3, 3, -2\rangle + 0.66\|1, 3, 3, 2\rangle$
1	8996	8974	22	$0.45\|1, 3, 4, 0\rangle - 0.51\|0, 4, 4, 0\rangle$
5	9021	8974	47	$-0.71\|1, 3, 3, -1\rangle + 0.30\|1, 3, 4, 3\rangle$
2	9025	—		$0.86\|1, 3, 3, 0\rangle$
5	9236	9175	61	$0.52\|1, 3, 3, -1\rangle - 0.50\|1, 3, 4, -1\rangle + 0.48\|0, 4, 4, -1\rangle$
4	9251	—		$0.37\|1, 3, 3, -2\rangle + 0.37\|1, 3, 3, 2\rangle + 0.42\|1, 3, 4, -2\rangle - 0.42\|1, 3, 4, 2\rangle$
2	9591	—		$0.42\|1, 3, 3, 0\rangle - 0.47\|1, 3, 4, -4\rangle + 0.47\|1, 3, 4, 4\rangle + 0.37\|0, 4, 4, -4\rangle$
1	9730	—		$0.43\|1, 3, 4, 0\rangle + 0.43\|1, 3, 4, -4\rangle + 0.43\|1, 3, 4, 4\rangle - 0.38\|0, 4, 4, 0\rangle$
3	9954	—		$0.52\|1, 3, 4, -2\rangle + 0.52\|1, 3, 4, 2\rangle - 0.39\|0, 4, 4, -2\rangle$
5	10 009	10011	−2	$0.33\|1, 3, 3, -1\rangle + 0.43\|1, 3, 4, -1\rangle + 0.52\|1, 3, 4, 3\rangle - 0.35\|0, 4, 4, -1\rangle$
4	11 064	—		$0.61\|1, 5, 6, -2\rangle - 0.61\|1, 5, 6, 2\rangle$
5	11 116	11 032	84	$0.64\|1, 5, 6, -1\rangle - 0.60\|1, 5, 6, 3\rangle$
1	11 133	—		$0.83\|1, 5, 6, 0\rangle - 0.34\|1, 5, 6, -4\rangle - 0.34\|1, 5, 6, 4\rangle$
3	11 631	—		$-0.67\|1, 5, 6, -2\rangle - 0.67\|1, 5, 6, 2\rangle$
5	11 741	—		$-0.64\|1, 5, 6, -1\rangle - 0.66\|1, 5, 6, 3\rangle$
2	11 794	—		$0.68\|1, 5, 6, -4\rangle - 0.68\|1, 5, 6, 4\rangle$
4	11 921	—		$0.65\|1, 5, 6, -6\rangle - 0.65\|1, 5, 6, 6\rangle$
3	11 973	—		$-0.64\|1, 5, 6, -6\rangle - 0.64\|1, 5, 6, 6\rangle$
1	12 056	—		$-0.46\|1, 5, 6, 0\rangle - 0.57\|1, 5, 6, -4\rangle - 0.57\|1, 5, 6, 4\rangle$
5	12 468	—		$0.93\|1, 5, 6, -5\rangle$
3	14 816	—		$0.34\|1, 1, 2, -2\rangle + 0.34\|1, 1, 2, 2\rangle - 0.50\|0, 2, 2, -2\rangle$
1	14 881	14 838	43	$-0.53\|1, 1, 0, 0\rangle - 0.43\|1, 3, 4, 0\rangle$
4	15 142	—		$-0.43\|1, 1, 2, -2\rangle + 0.43\|1, 1, 2, 2\rangle + 0.48\|0, 2, 2, -2\rangle$
5	15 277	15 182	95	$-0.55\|1, 1, 2, -1\rangle - 0.33\|1, 3, 2, -1\rangle$
1	15 508	15 517	−9	$0.45\|1, 1, 0, 0\rangle + 0.34\|1, 1, 2, 0\rangle - 0.49\|1, 3, 4, 0\rangle$
1	15 791	15 744	47	$-0.63\|1, 1, 0, 0\rangle + 0.43\|1, 1, 2, 0\rangle$
5	15 818	15 809	9	$0.56\|1, 3, 4, -1\rangle - 0.42\|1, 3, 4, 3\rangle + 0.53\|0, 4, 4, -1\rangle$
2	16 069	—		$0.43\|1, 3, 4, -4\rangle - 0.43\|1, 3, 4, 4\rangle + 0.50\|0, 4, 4, -4\rangle$
4	16 470	—		$-0.46\|1, 3, 4, -2\rangle + 0.46\|1, 3, 4, 2\rangle - 0.50\|0, 4, 4, -2\rangle$

Table 4. (Continued)

Γ	E^{a}_{calc} (cm^{-1})	E_{obs} (cm^{-1})	ΔE (cm^{-1})	Eigenvector
5	16 660	16 675	−15	$0.41\|1, 3, 4, -1\rangle + 0.52\|1, 3, 4, 3\rangle + 0.41\|0, 4, 4, -1\rangle$
1	16 719	16 675	44	$-0.34\|1, 3, 4, 0\rangle - 0.38\|1, 3, 4, -4\rangle - 0.38\|1, 3, 4, 4\rangle - 0.36\|0, 4, 4, 0\rangle$
3	17 094	—		$-0.43\|1, 3, 4, -2\rangle - 0.43\|1, 3, 4, 2\rangle - 0.52\|0, 4, 4, -2\rangle$
2	17 850	—		$-0.96\|1, 1, 1, 0\rangle$
5	18 300	18 281	19	$0.97\|1, 1, 1, -1\rangle$
5	19 670	19 696	−26	$0.79\|0, 6, 6, -1\rangle + 0.51\|0, 6, 6, 3\rangle$
1	19 682	19 738	−56	$0.82\|0, 6, 6, 0\rangle + 0.31\|0, 6, 6, -4\rangle + 0.31\|0, 6, 6, 4\rangle$
3	19 746	—		$-0.63\|0, 6, 6, -2\rangle - 0.63\|0, 6, 6, 2\rangle$
5	20 780	20 748	32	$-0.33\|0, 6, 6, -1\rangle + 0.66\|0, 6, 6, 3\rangle - 0.60\|0, 6, 6, -5\rangle$
2	20 793	—		$-0.67\|0, 6, 6, -4\rangle + 0.67\|0, 6, 6, 4\rangle$
4	20 869	—		$-0.66\|0, 6, 6, -2\rangle + 0.66\|0, 6, 6, 2\rangle$
5	21 340	—		$0.44\|0, 6, 6, -1\rangle - 0.46\|0, 6, 6, 3\rangle - 0.69\|0, 6, 6, -5\rangle$
1	21 428	—		$-0.47\|0, 6, 6, 0\rangle + 0.58\|0, 6, 6, -4\rangle + 0.58\|0, 6, 6, 4\rangle$
3	21 696	—		$0.45\|1, 1, 2, -2\rangle + 0.45\|1, 1, 2, 2\rangle + 0.31\|0, 2, 2, -2\rangle + 0.31\|0, 2, 2, 2\rangle$
4	22 018	—		$0.63\|0, 6, 6, -6\rangle - 0.63\|0, 6, 6, 6\rangle$
3	22 455	—		$0.32\|1, 1, 2, -2\rangle + 0.32\|1, 1, 2, 2\rangle - 0.54\|0, 6, 6, -6\rangle$
5	22 853	22 893	−40	$-0.76\|1, 1, 2, -1\rangle - 0.56\|0, 2, 2, -1\rangle$
4	23 024	—		$0.46\|1, 1, 2, -2\rangle - 0.46\|1, 1, 2, 2\rangle + 0.40\|0, 2, 2, -2\rangle$
1	23 204	23 241	−37	$0.77\|1, 1, 2, 0\rangle + 0.59\|0, 2, 2, 0\rangle$

[a] According to model A.
[b] Deduced from the thermally induced transitions at 5788 and 14 660 cm^{-1}.

Table 5. Final electronic structure parameters obtained for β-$ThGeO_4$ in comparison with the data published for $UGeO_4$ and $ThSiO_4$:U^{4+}. The values shown in square brackets were held fixed.

	β-$ThGeO_4$:U^{4+}		$UGeO_4$ [3]		
Parameter[a]	Model A	Model B	Model A	Model B	$ThSiO_4$:U^{4+} [2]
ζ (cm^{-1})	1809(12)	1802(11)	1767	1725	1840
F^2 (cm^{-1})	43 065(217)	42 330(363)	42 920	42 658	43 120
F^4 (cm^{-1})	38 977(1082)	35 623(964)	39 129	39 480	40 929
F^6 (cm^{-1})	24 391(793)	24 445(911)	27 753	24 448	23 834
α (cm^{-1})	34.7(2.1)	26(2.8)	22	29	32.3
$\beta/12$ (cm^{-1})	[−55]	[−55]	[−55]	−82	−55.3
γ (cm^{-1})	[1200]	[1200]	[1800]	[800]	[1200]
M^{0} [a] (cm^{-1})	[0.99]	[0.77]	[0.77]	[0.77]	—
P^{2} [b] (cm^{-1})	[500]	[500]	493	1970	—
B^2_0 (cm^{-1})	−1786	386	−1782	2918	−1003
B^4_0 (cm^{-1})	1204	−2327	2521	−2051	1147
B^4_4 (cm^{-1})	−3257	−6302	−3061	−3026	−2698
B^6_0 (cm^{-1})	−3165	−228	−3806	−487	−2889
B^6_4 (cm^{-1})	−994	−1161	−504	−1986	−208

[a] $M^2 = 0.56M^0$, $M^4 = 0.38M^0$ (after [10]).
[b] $P^4 = 0.5P^2$, $P^6 = 0.1P^2$ (after [15]).

the contributions originating from the M–O stretching and O–M–O bending. The electron–phonon coupling for these modes are especially efficient.

The calculated levels 11 741, 12 056, 12 468, 21 340 and 21 428 cm^{-1} are not observed in the spectrum. As for the first three levels it is a characteristic feature of the U^{4+} optical

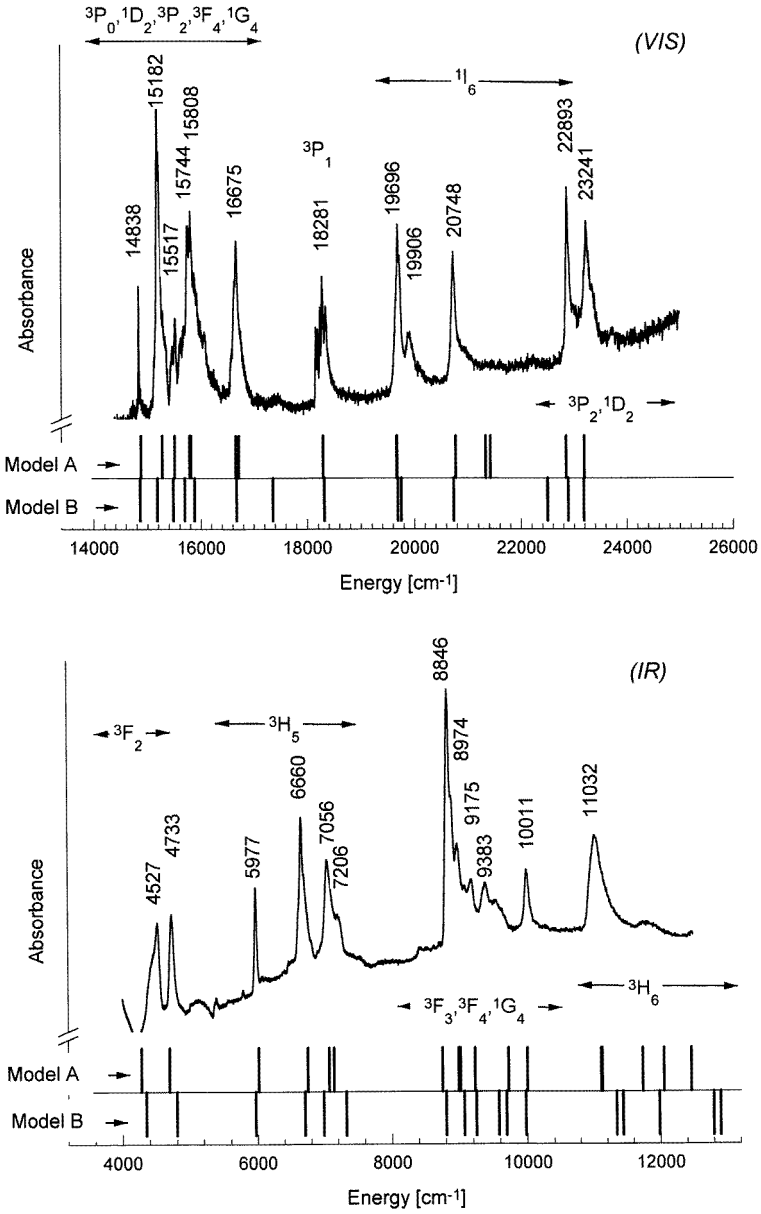

Figure 2. Absorption spectra of β-$ThGeO_4$:U^{4+} and positions of calculated levels (models A and B) allowed by the selection rules shown in table 1.

spectra that the $^3H_4 \rightarrow {}^3H_6$ transitions have in general a low (close to zero) intensity. For the remaining two levels we have no explanation apart perhaps from the fact that it is quite a common failure.

The spin–orbit coupling constant ζ and the Slater integrals F^k are in excellent agreement with the CPM prediction. Also the crystal-field parameters of the fourth order are convergent with the theoretical estimation. It is easy to check that these parameters play an essential role in the whole crystal-field effect.

In the case of B_0^2 and B_4^6 we observe a large discrepancy. The unpredictability of these parameters in the case of tetragonal matrices of D_{2d} symmetry is not unusual [1]. In principle, B_0^2 and B_4^6 should have relatively small values resulting from the above-mentioned competition of the two coordination tetrahedra. Such a picture may be changed, however, if we take into account, apart from the uranium position variation, the influence of the higher-order induced multipoles. From table 3 we see that the contribution of the induced dipoles to B_0^2 is very large. Unfortunately, there are no reliable data of the higher-order polarizabilities of the ions. More precisely, we have checked that the multipole expansion in which we apply the theoretically evaluated polarizabilities is not convergent. Probably the polarizabilities calculated for the free ions are overestimated. It does not concern the dipolar polarizability for which more reliable experimental data are available.

From the viewpoint of the accuracy of the experimental data fits the B_0^2 parameter is very sensitive to the exact position of levels such as $^3P_1(\Gamma_2)$ and $^3P_1(\Gamma_5)$. The energy of these level depends on B_0^2 but also on F^k and ζ. This means that the accuracy of determination of B_0^2 from these particular levels remains closely related to the accuracy of determination of the free-ion parameters the effect of which is in principle one order larger.

The remaining crystal-field parameters in model A are consistent not only with the FPPM calculations but also with the results obtained for the uranium ion doped in the other thorite matrix β-$ThSiO_4$ [2] and one of the models (thorite model A) discussed for $UGeO_4$ [3]. As we noted in the previous section, model B gives the crystal-field parameters convergent with the FPPM calculations for U^{4+} in the scheelite matrix α-$ThGeO_4$. We see from figure 1 that the thorite (β-$ThGeO_4$) and scheelite ($UGeO_4$) matrices do provide similar energy patterns despite large differences in the crystal-field parameters (see table 5). The fits of the data recorded for $UGeO_4$ also led to two different parameter sets [3]. The above arguments point to the scheelite model (also denoted B in [3]) as more appropriate for the uranium germanate.

6. Conclusions

The infrared and visible absorption spectra of the U^{4+} ion in the tetragonal matrix β-$ThGeO_4$ of thorite structure have been recorded at various temperatures and interpreted in terms of the conventional phenomenological approach. The results are consistent with the initial theoretical predictions and the previous results obtained for β-$ThSiO_4$. The existence of several, only slightly different non-equivalent uranium positions has been stated. The most apparent dependence of the energy of $\Gamma_5(^3P_1)$ level on the uranium position has been attributed to the specific character of the B_0^2 crystal-field parameter in the crystalline matrix under study. We have noted an ambivalence of the uranium electronic structure deduced from the spectroscopic data similar to that reported for $UGeO_4$ of scheelite structure. The final choice is determined by the theoretical estimation of the crystal-field effect.

References

[1] Krupa J C 1987 *Inorg. Chim. Acta.* **139** 223
[2] Khan Malek C and Krupa J C 1986 *J. Chem. Phys.* **84** 6584
[3] Gajek Z, Krupa J C, Żołnierek Z, Antic-Fidancev E and Lemaitre-Blaise M 1993 *J. Phys.: Condens. Matter* **5** 9223
[4] Crosswhite H M and Crosswhite H 1984 *J. Opt. Soc. Am.* B **1** 246
[5] Carnall W T and Crosswhite H M 1985 *Argonne National Laboratory Report* ANL-84-90
[6] Gajek Z, Mulak J and Faucher M 1987 *J. Phys. Chem. Solids* **48** 947
[7] Gajek Z and Mulak J 1992 *J. Phys.: Condens. Matter* **4** 947

[8] Ennaciri A, Kahn A and Michel D 1986 *J. Less-Common Met.* **124** 105
[9] Schoenes J 1980 *Phys. Rep.* **63** 301
[10] Judd B R, Crosswhite H M and Crosswhite H 1968 *Phys. Rev.* **169** 130
[11] Ng B and Newman D J 1985 *J. Chem. Phys.* **83** 1758
[12] Gajek Z 1995 *J. Alloys Compounds* **219** 238
[13] Newman D J and Ng B 1989 *J. Phys.: Condens. Matter* **1** 1613
[14] Gajek Z, Lahalle M P, Krupa J C and Mulak J 1988 *J. Less-Common Met.* **139** 351
[15] Carnall W T, Liu G K, Williams C W and Reid M F 1989 *J. Chem. Phys.* **95** 7194
[16] Khan Malek C, Krupa J C, Delamoye P and Genet M 1986 *J. Physique* **47** 1763
[17] Vaderborre M T, Michel D and Ennaciri A 1989 *Spectrochimica Acta.* A **45** 721